e-ISSN: 2637-0611

Available online at
https://journal.uitm.edu.my/ojs/index.php/COS

Compendium of Oral Science 12 (2) 2025, 122 - 153

Compendium of Oral Science

Modified Method for Synthesis of Microwave-Assisted Irradiation Hydroxyapatite for Alveolar Ridge Preservation

Nurul Saadah Razali[2], Luay Thanoon Younis[1]*, Muhammad Hilmi Zainal Ariffin[1], Fara Fariza Zahar[1]

[1]*Faculty of Dentistry, Universiti Teknologi MARA Sungai Buloh Campus, Jalan Hospital, 47000 Sungai Buloh, Selangor, Malaysia*
[2]*Periodontic Unit, Mahmoodiah Dental Clinic, Ministry of Health, 80100 Johor Bahru, Malaysia*

ARTICLE INFO

Article history:
Received 03 November 2024
Revised 06 January 2025
Accepted 06 March 2025
Online First
Published 01 September 2025

Keywords:
hydroxyapatite
microwave-assisted
alveolar ridge

DOI:
10.24191/cos.v12i2.8835

ABSTRACT

Hydroxyapatite is one of the commonly used alloplastic material for alveolar bone regeneration. However, the currently practiced methods of synthesis are often time-consuming. The commercially available hydroxyapatite, even though were proven to attenuate alveolar bone resorption, they also showed a low biodegradability. This study is aimed to describe a new method of synthesising hydroxyapatite using microwave-assisted irradiation method.

Methods: 52g Calcium nitrate tetrahydrate was dissolved in 5% hydrogen peroxide until it completely dissolved. Stoichiometric amount of 85% phosphoric acid were added dropwise, and the pH of the suspension was adjusted using ammonium hydroxide solution. The suspension was continuously stirred for additional 30 minutes at the room temperature. One part of the suspension was heated in household microwave at 800W for 10 minutes. Another half was filtered and washed using distilled water (named as filtration-HAp). Each suspension was further freeze-dried and calcined at 600C for 2 hours. The obtained powders were further characterised by using x-ray diffractometer, fourier transform infrared spectroscopy and energy dispersive x-ray fluorescence. Morphology of obtained powders were observed using field emission electron microscope.

Results: X-ray diffraction pattern of microwave-HAp showed high peaks indicating a highly crystalline structure. FTIR results confirms the presence of phosphate and hydroxyl groups. EDXRF showed calcium-to-phosphorus ratio of 1.8. Microwave-HAP showed non-homogenous

[1*] Corresponding author. *E-mail address*: drluay@uitm.edu.my

spherical shape with less agglomeration, whereas filtration-HAP showed amorphous and highly agglomerated structure.

Conclusions: Microwave-assisted irradiation method enables the rapid synthesis of pure hydroxyapatite nano powder with high crystallinity. The modified microwave-HAp can be considered a potential bone substitute. Further in-vivo investigations are required to ascertain the desirable mechanical properties and optimal concentration of MW-Hap for tissue biocompatibility.

1. INTRODUCTION

Alveolar bone regeneration is an essential aspect in treating periodontal diseases, placing dental implants, and prosthetic rehabilitation. Periodontal diseases often begin with an inflammatory response caused by bacteria in the subgingival biofilm, which leads to damage in tissues supporting the teeth. Although non-surgical treatments can reduce inflammation, they usually do not fully restore the damaged tissues, leading to weakened tooth support that requires tooth extraction and possibly leads to bone defects in the jaw (Meyle & Chapple, 2015). For enhancing periodontal stability and extending tooth lifespan, a method known as guided tissue regeneration is applied. This technique frequently incorporates the use of membranes to serve as barriers against the downward growth of epithelial cells, and bone grafts are utilised to provide a structural scaffold (Cortellini & Tonetti, 2015). However, in advanced cases, periodontitis often results in tooth loss, necessitating teeth replacement by dental implants and other prostheses to regain chewing function and improve aesthetic appearance. Therefore, adequate alveolar ridge dimension is a crucial aspect of achieving the goals. Perhaps the preservation of the alveolar ridge dimension during the time of extraction and reconstruction of the previously resorbed alveolar ridge could be applied, but both methods critically need biomaterials to enhance new bone formation. Over the years, there has been extensive research and development in the fields of regenerative medicine and biomaterials to produce a reliable and predictable method to promote alveolar bone regeneration.

Regenerative medicine and tissue engineering offer a promising approach to promoting tissue regeneration and constructing patient-specific needs for teeth replacement. These methods involve the use of diverse therapies, such as bone graft (autogenous, allogenic, xenogenic or alloplastic), bioactive factors (enamel matrix derivatives and various growth factors), stem cells and gene therapy (Larsson et al., 2015). The clinical efficacy of these biomaterials, either used alone or in combination, has been investigated in systematic reviews and meta-analyses (Meyle & Chapple, 2015; Sanz-Sánchez et al., 2015). None of these biomaterials were considered 'the best biomaterial' compared to one another.

In the context of maintaining and restoring alveolar bone dimensions, bone grafts remain a fundamental biomaterial owing to their ability to offer scaffolding and mechanical support. Moreover, the existence of a scaffold is crucial for guiding cell behaviour towards appropriate phenotypes in connective tissue, providing both biological and structural support for the regeneration process. Numerous research efforts have concentrated on developing bone graft materials that fit each clinical application. An autograft is a bone taken from one side of an individual and transplanted to another site in the same person, which has historically been regarded as the ideal bone grafting material. This is because it naturally contains all the essential elements for bone formation: osteogenic cells (stem cells), osteoinductive agents (growth factors), and osteoconductive structures (scaffolds).

Conversely, an allograft, tissue obtained from a different human donor, offers the advantage of not increasing surgical complexity, a typical limitation of autografts. Allografts are frequently used in bone regeneration with a relatively low risk of disease transmission, thanks to thorough screening processes,

https://doi.org/10.24191/cos.v12i2.8835

tissue processing techniques, and methods for eradicating viruses. Xenografts, derived from animal sources such as pigs and cows, have also shown effectiveness in reducing the loss of alveolar bone. These grafts undergo thermal and chemical processing to minimise their antigenicity, reducing immune rejection risk. However, these processes often strip away the osteogenic and osteoinductive potential of the grafts, leaving behind only their osteoconductive capabilities. An emerging alternative is the use of alloplastic materials like hydroxyapatite, bioactive glass, octacalcium phosphate, and tricalcium phosphate (TCP). These synthetic materials are engineered to mimic the natural bone environment, offering the advantage of being readily available and having controllable properties (Sano et al., 2023).

As synthetic materials, alloplasts offer superiority in their wide-ranging availability, ease of use, and capacity to avoid surgery to obtain donor tissue. Similar to other bone grafts, they serve as a framework for the growth of cells required for bone regeneration (osteoconductive), stimulate the multiplication and migration of bone-forming cells (osteoinductive), and can incorporate living cells capable of generating new bone tissue (osteogenic). Among various alloplastic substances, hydroxyapatite (HAp) is frequently used due to its excellent bioactivity, biocompatibility and osteoconductive characteristics. Hydroxyapatite is one of the primary substitute materials grouped under the calcium phosphate ceramic group that has been widely employed in surgical procedures for bone regeneration. The composition of bone consists of approximately 69% by weight of mineral apatite, 22% by weight of organic components such as matrix proteins, lipids, and osteogenic substances, and 9% by weight of water. The mineral constituents of bone are recognised as calcium hydroxyapatite, with non-uniformly formed particles with dimensions ranging from 30 to 45 nm in length and width and an average thickness of approximately 5 nm. Synthetic HAp, with the chemical formula $Ca_{10}(PO_4)_6(OH)_2$, exhibits a calcium phosphate ratio of 1.67, which closely resembles the mineral constituents found in bone tissue (Rajula et al., 2021).

The key benefit of HAp lies in its osteoconductive properties for alveolar bone regeneration. It has been proven in various studies that the bioactive properties of HAp were able to act as a temporary space for cell adhesion and proliferation, thus facilitating early bone healing, demonstrated histologically by increased new bone formation with less connective tissue component. With regards to the ability to maintain structural alveolar bone integrity, HAp showed a favourable outcome in minimising the alveolar bone resorption after extraction comparable to xenograft. As the chemical formula of synthetic HAp resembles the bony apatite structure, the inquiry of its biocompatibility is no longer a concern. (Kattimani et al., 2019).

Previously, conventional methods of producing HAp yielded a large particle size-to-volume ratio, limiting its use in biomedical applications. Nowadays, the understanding of nanotechnology has led to a unique approach to overcoming the shortcomings of conventional HAp. Nanocrystalline HAp was shown to exhibit osteoinductive properties due to its ability to stimulate the host mesenchymal stem cells to differentiate into osteoblasts. The exact mechanism of bone induction is still unclear, but the increased chemotactic cell activity is believed to be facilitated by a conducive environment provided by an appropriate geometry, topography and microporosity of HAp. The enhanced properties of nanosized HAp have also been demonstrated in terms of better dissolution and resorbability than conventional HAp due to the smaller particle size. This biodegradability rate is important for creeping resorption to take place during the bone healing process, allowing new bone formation to occur (Islam et al., 2020; Kattimani et al., 2016).

Another crucial component to be considered in searching for suitable biomaterial for oral use is the optimum mechanical strength. HAp has low fracture toughness, limiting its use in high occlusal load areas. Alternatively, HAp was incorporated with other substances to improve its properties. The ability of HAp to chemically combine with various organic and inorganic substances, forming biomaterial composites, making its application more versatile in the field of regenerative medicine. Furthermore, the mechanical properties of HAp depend on the pore interconnectivity, crystal size, phase composition and density.

https://doi.org/10.24191/cos.v12i2.8835

Therefore, the control of characteristic features can be made possible only by synthetic processes, allowing to modulate mechanical and biological behaviour is the answer to (Wang et al., 2014). Owing to the versatility of this material, it is valuable to investigate the development of a novel form of HAp designed to meet all criteria for bone regeneration at specific locations. There have been initiatives aimed at creating an ideal product that is customised for distinct clinical uses, either by altering current production methods or inventing new synthesis techniques. Despite these efforts, a material that completely satisfies all requirements for bone regeneration has yet to be discovered.

2. MATERIALS AND METHODS

2.1 Materials

The materials used to synthesize both HAp in this study comprised five chemical reagents:

- Calcium nitrate tetrahydrate (Sigma Aldrich, 0.25 mol)
- Hydrogen peroxide 30% (Sigma Aldrich)
- Distilled water
- Phosphoric acid 85% (Merck)
- Ammonium hydroxide (Sigma Aldrich)

2.2 Microwave calibration

Microwave calibration was done by putting 500 grams of distilled water inside a beaker. The water was heated using lower microwave power, starting from 100 Watts until 900 Watts for 10 minutes. The temperature of the water was recorded using a fibre optic sensor (García-Baños et al., 2019). The water temperature was matched with the theoretical temperature using the following formula:

$$T_f = T_i + mcQ$$

Where,
T_i = Initial temperature (°C)
Q = heat energy
m = mass of water (kg)
c = specific heat capacity of water (4190 J/(kg·°C)

2.3 Synthesis methods

2.3.1 Synthesis of Microwave-Irradiation Hydroxyapatite

The pure HAp was prepared using simple and clean methods. 59.0 grams of calcium nitrate tetrahydrate (Sigma Aldrich, 0.25 mol) was dissolved into 25 ml of 30% V/V hydrogen peroxide (Sigma Aldrich) and 125 ml distilled water in a 500 ml pyrex beaker. After the particles were completely dissolved, a stoichiometric amount of 85% phosphoric acid (Merck) was added dropwise with continuous stirring. The following calculations were followed to determine the amount of phosphoric acid needed to react with 52 grams of calcium nitrate tetrahydrate to produce HAp in a stoichiometric manner.

https://doi.org/10.24191/cos.v12i2.8835

The molecular weight of the reactants is as follows:

Calcium nitrate tetrahydrate:

$(Ca(NO_3)2{\cdot}4H_2O)$ = 40.08 (Ca) + 2x(14.01 (N) + 3x16.00 (O)) + 4x(2x1.01 (H) + 16.00 (O)) = 236.15 g/mol

Phosphoric acid:

(H_3PO_4) = 3x1.01 (H) + 30.97 (P) + 4x16.00 (O) = 98.00 g/mol

The balanced chemical equation for the formation of HAp:

$5Ca(NO_3)_2{\cdot}4H_2O + 3H_3PO_4 + NH_4OH \rightarrow Ca_5(PO_4)_3(OH)$ + Other Products

The stoichiometric relationship from the equation shows that 5 moles of calcium nitrate tetrahydrate react with 3 moles of phosphoric acid. Thus, the moles of calcium nitrate tetrahydrate were:

Moles of $Ca(NO_3)_2{\cdot}4H_2O = \frac{Mass}{Molar\ mass} = \frac{52\ g}{236.15\ g/mol}$

Then, using the stoichiometry from the chemical equation (5 moles of $Ca(NO_3)_2{\cdot}4H_2O$ to 3 moles of H_3PO_4), the moles of H_3PO_4 needed:

Moles of H_3PO_4 = Moles of $5Ca(NO_3)2{\cdot}4H_2O$ x $\frac{3}{5}$
$= \frac{52\ g}{236.15\ g/mol}$ x $\frac{3}{5}$
= 0.132 mol

Mass of H_3PO_4 = Moles of H_3PO_4 x molar mass of H_3PO_4
= 0.132 mol x 98.00 g/mol
=12.95 g

Thus, the amount of phosphoric acid needed to react with 52 grams of calcium nitrate tetrahydrate is approximately 12.95 g.

To determine the volume of 85% phosphoric acid required:

$$\text{Volume} = \frac{Mass\ of\ H3PO4}{Density\ x\ Percentage\ concentration}$$

Where:
Mass of H_3PO_4 – 12.95 g
Density of 85% H_3PO_4 = 1.684 g/ml
Percentage concentration = 0.85

The final volume of 85% phosphoric acid needed was 9.04 ml.

https://doi.org/10.24191/cos.v12i2.8835

After 9.04 ml of 85% phosphoric acid was added, ammonium hydroxide solution (Sigma Aldrich) was then added to produce the white precipitate until the pH reached 10. The suspension was then stirred continuously at room temperature for an additional 30 minutes until the suspension became homogenous. To prepare the microwave HAp, the beaker was covered with a silicone perforated tray (Fig. 1). Then, the suspension was heated in a microwave oven (Panasonic NN-ST25JBMPQ 20L) at 800 watts for 10 minutes (Fig. 2). The obtained suspension was freeze-dried. All the powder was calcined at 600°C for 2 hours (Fig. 3).

The experiments were repeated by adjusting the amount of phosphoric acid until the optimum Ca/P ratio was obtained.

Fig.1. Suspension inside the microwave covered with perforated silicone sray.

https://doi.org/10.24191/cos.v12i2.8835

Fig. 2. Microwave used to synthesise hydroxyapatite.

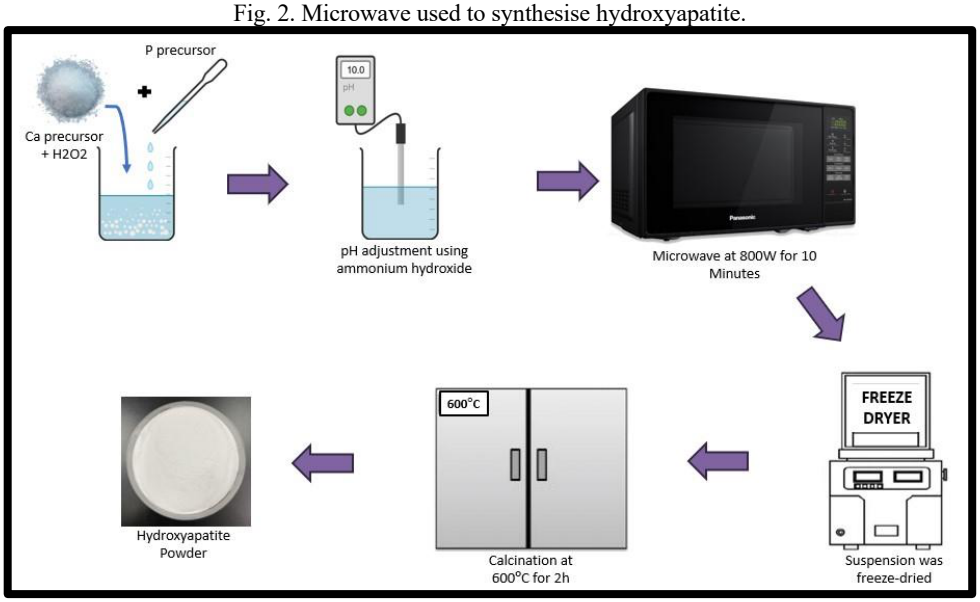

Fig.3. Steps in the synthesis of hydroxyapatite using microwave-irradiation method.

2.3.2Synthesis of Filtration-Hydroxyapatite

The control powder (f-HAp) was prepared using the same methods above but without the use of a microwave, according to the method described by Lamkhao et al. 2019. Only one stoichiometric HAp was prepared. Accordingly, 59.0 grams of calcium nitrate tetrahydrate (Sigma Aldrich, 0.25 mol) was dissolved into 25 ml of 30% V/V hydrogen peroxide (Sigma Aldrich) and 125 ml distilled water using 500 ml pyrex beaker. After the particles were completely dissolved, a stoichiometric amount of 85% phosphoric acid (9.04 ml) was added dropwise with continuous stirring. After obtaining the homogenous solution after 30 minutes of stirring, the suspension was filtered (Fig. 4), washed, and calcined at 600°C for 2 hours (Lamkhao et al., 2019).

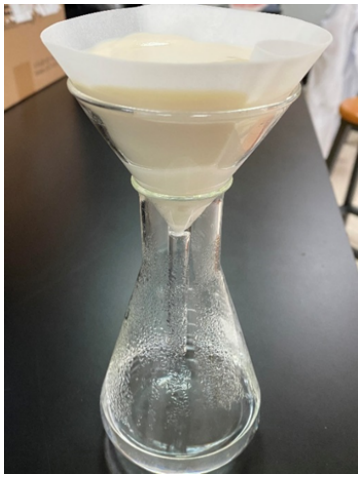

Fig.4. Filtration process to obtain f-HAp

2.4 Characterization of Hydroxyapatite powder

2.4.1 Preliminary analysis of Calcium-to-Phosphorus ratio

X-ray Diffraction Fluorescence Spectroscopy (EDXRF) was used as an analytical tool in the determination of the Ca/P ratio. This method was chosen due to its non-destructive nature and high sensitivity to elemental composition.

In this study, the application of EDXRF involves subjecting HAp samples to X-ray excitation, inducing the emission of characteristic X-rays from the material. These emitted X-rays are then dispersed and detected, allowing for the identification and quantification of elements present in the sample. Given its non-destructive nature and high sensitivity to elemental composition, EDXRF proves to be well-suited for precisely assessing the Ca/P ratio in HAp.

The methodology commences with the preparation of HAp samples, ensuring their homogeneity and representative nature. Following this, the samples undergo EDXRF analysis within controlled experimental parameters. Two parameters were controlled in the instrument settings, including excitation energy and detection parameters, and were performed to heighten the accuracy and precision of determining the Ca/P ratio. Calibration standards comprising well-defined Ca/P ratios are done to establish a correct correlation between X-ray intensities and elemental concentrations.

For each sample, the measurements were done three times. The obtained EDXRF spectra are then processed using Epsilon3-XL software to extract elemental information and calculate the average Ca/P ratio. The data is presented in the form of the weight percentage of each element. The mw-HAp that has the optimum Ca/P ratio was used for further analysis.

2.4.2 X-ray Diffraction Pattern

X-ray diffraction is a fundamental technique used in various scientific disciplines to analyze the structure of crystalline materials. It is widely employed in materials science, physics, chemistry, and biology for its ability to provide detailed information about the arrangement of atoms within a crystal lattice. X-ray diffraction, which is a non-destructive technique, involves the scattering of X-rays by the regularly spaced atoms in a crystal, resulting in the formation of a diffraction pattern that can be analyzed to provide information about the internal structures within the range of 0.1 to 100 nm (Holder and Schaak 2019).

The X-ray diffractometer's capacity to describe a material's crystal structure makes it an invaluable instrument for HAp identification. Hence, this method has been extensively used to examine the distinct crystalline structure and phase purity of HAp, an essential component of bone and teeth. It also provides important information about crystal composition, arrangement of atoms, adsorptive properties and crystallographic alteration under different conditions. It can also be employed in characterising HAp obtained from diverse sources, such as dromedary bone and crab shells (Ghedjemis et al. 2021; Raya et al. 2015).

https://doi.org/10.24191/cos.v12i2.8835

The principle behind the determination of the peak position of each material analyzed using this technique is based on Bragg's Law expressed as:

$$2d.\sin\theta = n\lambda$$

where,
d = interatomic distance
θ = path difference between the incident ray and diffracted ray
n = integer (the order of incidence)
λ = wavelength of the incident x-rays

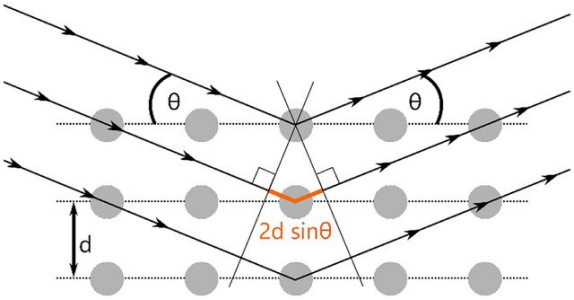

Fig.5. Schematic diagram for visualization of Bragg's Equation
(Harrington & Santiso, 2021)

When the X-ray falls on the rotating target in the X-ray diffractometer, x-ray energy becomes diffracted and detected through a detector containing a photomultiplier tube, producing an XRD pattern. Each peak in the XRD pattern corresponds to a crystallographic plane set that satisfies Bragg's Law for a particular angle (2θ). The smaller 2θ value indicates a larger interplanar spacing, and vice versa. The 2θ values of diffraction peaks are unique for each crystallographic phase (Fig. 5). Using this way, determination of the crystalline phases present in a material was possible by conducting a comparative analysis of the peak positions observed in an experimental XRD pattern with the reference patterns available in databases (Otwinowski and Minor 1997).

The powders in this study were identified by comparing them with a known reference pattern utilising data obtained from the International Crystal Structure Databases (Refer Appendix A). To determine the phase of the material, the peak position (2θ) and intensity were compared, ensuring that they were equal. This analysis aimed to distinguish whether the material was in a single phase or amorphous state. In addition, the d-spacing of the lattice plane (hkl) and average crystallite size were also calculated by measuring the area of diffraction peaks using Scherrer equation (Bilton, 2012):

$$\tau = \frac{\kappa\lambda}{\beta \cos\cos\theta}$$

where,
κ = shape factor
λ = x-ray wavelength

https://doi.org/10.24191/cos.v12i2.8835

β = full width of diffraction peak at the half of maximum intensity (FWHM) in radians
θ = path difference between the incident ray and diffracted ray

The obtained samples were characterised using an X-ray diffractometer (PANalytical X' Pert PRO MPD System) using a Cu-Kα radiation source. Diffraction patterns were collected in a range $2\theta/\theta$ scanning mode at 40 kV and 20 mA. Then, crystalline size and lattice parameters were calculated based on the obtained XRD pattern by using the software Origin 2023.

2.4.3 Fourier Transform Infrared Spectroscopy (FTIR) Analysis

This is a highly effective method for identifying and characterizing organic and certain inorganic compounds by examining their molecular vibrations. The fundamental process involves measuring the absorption of infrared radiation by a sample, where the absorbed frequencies correspond to the vibrational frequencies of the chemical bonds present. In the FTIR instrument, an interferometer modulates the infrared radiation, and the resulting interferogram is fourier-transformed to produce an infrared spectrum. This spectrum reveals absorption peaks at distinct wavelengths, indicating specific vibrational modes associated with different chemical bonds and functional groups. Analysts can interpret the FTIR spectrum to identify functional groups and deduce molecular structures based on known absorption frequencies. FTIR offers detailed insights into the chemical composition and interactions within samples, making it a standard tool in laboratories for both qualitative and quantitative analyses (Peak, 2005).

In Fourier-transform infrared spectroscopy (FTIR), the infrared wavelength (λ) is commonly expressed as wavenumber ($\bar{\upsilon}$), which is the inverse of the wavelength in cm^{-1}. The mid-IR wavenumber range typically spans from 4000 to 400 cm^{-1}, where an increase in wavenumber corresponds to higher energy (E). The energy (E) is calculated using the equation.

$$E = hc\bar{\upsilon},$$

Where,
h = Planck's constant (6.6×10^{-34} J s^{-1})
c = the speed of light (3×10^{10} cm s^{-1}).

Functional groups were analysed within the samples using a Perkin Elmer FTIR spectrometer equipped with PerkinElmer Spectrum software (Fig. 6). For sample preparation in this study, 1 mg of the sample was ground with 100 mg of KBr using a pellet press. Fourier-transform infrared spectroscopy was employed with a model featuring a resolution of 4 cm^{-1}, analyzing an average of 32 images within the wavenumber range of 4000-400 cm^{-1}.

https://doi.org/10.24191/cos.v12i2.8835

Fig.6. Perkin Elmer FTIR Spectrometer

2.4.4 Agglomeration and morphology

The agglomeration and HAp morphology were observed using a Field Emission Scanning Electron Microscope (FE-SEM), JSM-7600F by JEOL (Fig. 7). The HAp samples were prepared by mounting the powder into an SEM stub using double-sided carbon tape. The mounted powder was inspected to ensure a uniform, thin layer to facilitate beam penetration. Then, the mounted powder was coated with gold using the sputter coater.

Experimental parameters, such as accelerating voltage, working distance, and detector settings, are carefully optimized to achieve the desired image quality. The images were then captured starting at the lower magnification and gradually increasing the magnification until the maximum of 200 nm. The images obtained were then analyzed to determine the agglomeration state and morphological characteristics of the HAp.

https://doi.org/10.24191/cos.v12i2.8835

Fig.7. Field Emission Scanning Electron Microscope (FESEM)

3. RESULTS

HAp is a crucial biomaterial in various biomedical applications, particularly for alveolar bone reconstruction. Its synthetic route synthesis is favoured for its simplicity and control over the key reaction parameters. In the realm of bone regeneration, the effectiveness of nanoscale HAp hinges on several factors, such as purity, morphology, and the calcium-to-phosphorus (Ca/P) ratio, which can be tailored to meet specific requirements. This investigation successfully synthesized a novel mw-HAp that exhibits superior physical properties in comparison to f-HAp.

The study also revisits the physical characteristics and antibacterial effectiveness of f-HAp, confirming alignment with previous findings by Lamkhao et al. (2019), notwithstanding a slight deviation in the Ca/P ratio. Notably, this research extends the knowledge base by examining the effects of f-HAp on the viability and proliferation of human osteoblast cells, which has not been previously investigated.

The results discussed herein encompass the optimum calcium-to-phosphorus ratio, phase composition, crystallinity, morphology, antibacterial activity and cytotoxicity, as determined through a series of analytical techniques.

3.1 Synthesis of Hydroxyapatite

The primary aim of this investigation was to evaluate the potential of microwave irradiation in the synthesis of HAp with distinctive properties, potentially outperforming those produced through previous methods in aspects such as crystallinity, particle size, mechanical properties, antibacterial activity, and cytotoxicity (as discussed from sections 4.3 to 4.9).

The methods used in the synthesis of mw-HAp involve mixing the precursors, pH adjustment, microwave irradiation, freeze-drying, and calcination. For the f-HAp, after the pH adjustment, the suspension was filtered and washed using distilled water. A few reaction parameters were controlled,

https://doi.org/10.24191/cos.v12i2.8835

including microwave power, pH and stirring time. Notably, mw-HAp synthesis significantly reduces preparation time, as it eliminates the need for filtration and washing, yielding a highly pure powder.

Figure 7 shows the HAp produced by the two methods. Both HAp syntheses' chemical reactions are placed below, with some impurities present. The impure compounds were detected using the previously mentioned EDXRF and FTIR analysis.

$$5Ca(NO3)2{\cdot}4H2O + 3H3PO4 + NH4OH \rightarrow Ca5(PO4)3(OH) + \text{Other Products}$$

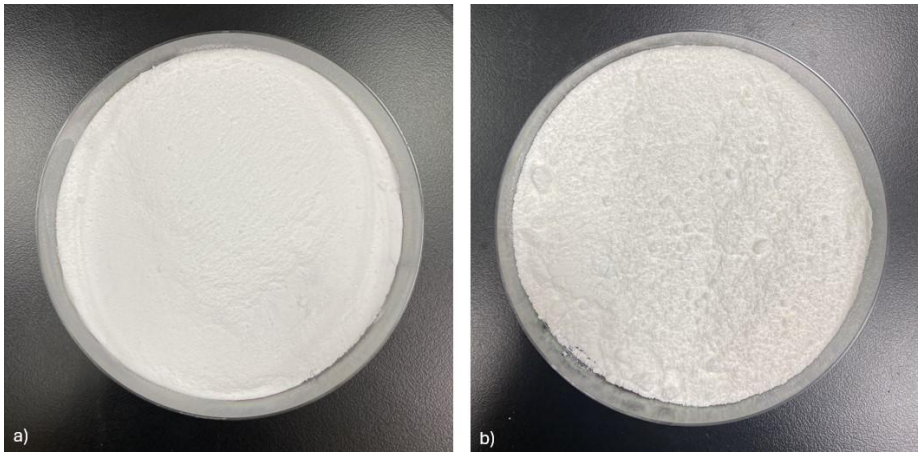

Fig.8. a) microwave-HAp powder, b) filtration-HAp powder

3.2 Preliminary Analysis of Calcium-to-Phosphorus Ratio

The stoichiometric HAp was initially obtained by mixing calcium and phosphate precursors in a 10:6 ratio. A preliminary analysis of the optimum amount of phosphate precursor to react with the specific amount of calcium nitrate tetrahydrate was conducted first, and EDXRF determined the calcium-to-phosphorus ratio (Table 1). The experiments were conducted with the control of other variables, including microwave power, pH, stirring time, ageing time and sintering time. Using the microwave-irradiation method, the optimum Ca/P ratio was 1.8, which can be obtained by adding 30% higher amounts of phosphoric acid needed from the actual stoichiometric amount. Adding lesser or higher amounts of phosphate precursors leads to a higher Ca/P value that could be due to unreacted calcium. Thus, this study found that obtaining an exact calcium phosphate ratio of 1.67 is almost impossible. With regards to the f-HAp, the optimum Ca/P was also 2.0, even though the stoichiometric amount of calcium and phosphorus ratio was used. In comparison with the other group of researchers, they found a Ca/P ratio of 1.72 after using the exact method (Lamkhao et al., 2019). The Ca/P ratio was intentionally altered by adjusting the phosphorus content relative to the calcium in the initial solution to accelerate the nucleation process of HAp during its crystallization phase. It was observed that an environment with a higher concentration of calcium facilitated quicker nucleation of HAp, resulting in the formation of HAp particles that were smaller in size (Kim et al., 2004).

https://doi.org/10.24191/cos.v12i2.8835

Table 1. EDXRF spectra for the powder obtained from microwave-assisted irradiation method.

Calcium nitrate tetrahydrate (g)	Phosphoric acid volume (ml)	Average of weight percentage of Ca (%)	Average weight percentage of P (%)	EDXRF Ca/P ratio
52	8.00	54.81	10.34	4.1
52	9.00	54.09	11.95	3.5
52	10.00	49.52	14.38	2.7
52	11.00	53.61	15.8	2.6
52	12.00	48.5	20.79	1.8
52	15.00	50.45	18.84	2.1
52	16.00	49.71	17.34	2.2
52	17.00	47.87	18.2	2.1
52	18.00	42.11	14.32	2.3

3.3 X-ray Diffraction Pattern Analysis

The X-ray diffraction pattern was determined for powders obtained from both methods. The XRD pattern for the powder obtained from the microwave-assisted irradiation method shows the HAp characteristic comparable with the ICDD data with reference code 01-074-0566 (Sudarsanan & Young, 1969). The sharp and high intensity peaks are identified at 25.9°, 28.3°, 31.6°, 33.0°, 34.9°, 44.2°, 47.5°, 48.7°, 51.9°, and 53.5°. These peaks give the HKL values of 002, 102, 211, 300, 202, 130, 222, 213, and 004 respectively (Fig. 9). The sharp peaks suggest a well-ordered crystal structure. The calculated crystal size shows an average size of 33 nm. The crystallinity of this powder was 98.6%.

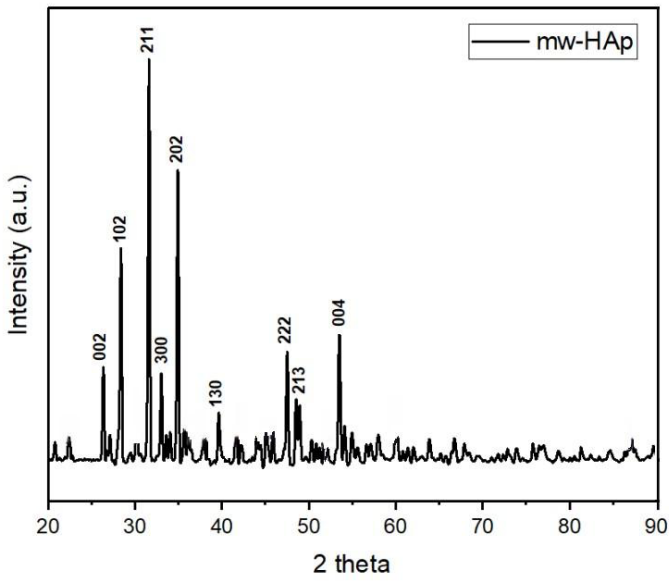

Fig.9. XRD pattern of mw-HAp

https://doi.org/10.24191/cos.v12i2.8835

XRD pattern of the powder obtained from the filtration method shows peaks located at 25.9°, 31.9°, 39.7°, 46.6°, 49.6°, and 53.3°. The peak locations are corresponded to HKL values of 002, 211, 130, 222, 213 and 004 (Fig. 10). The broader peaks with lower intensity are observed for this powder. The calculated particle size is 12.3 nm, with a crystallinity of 41.1%.

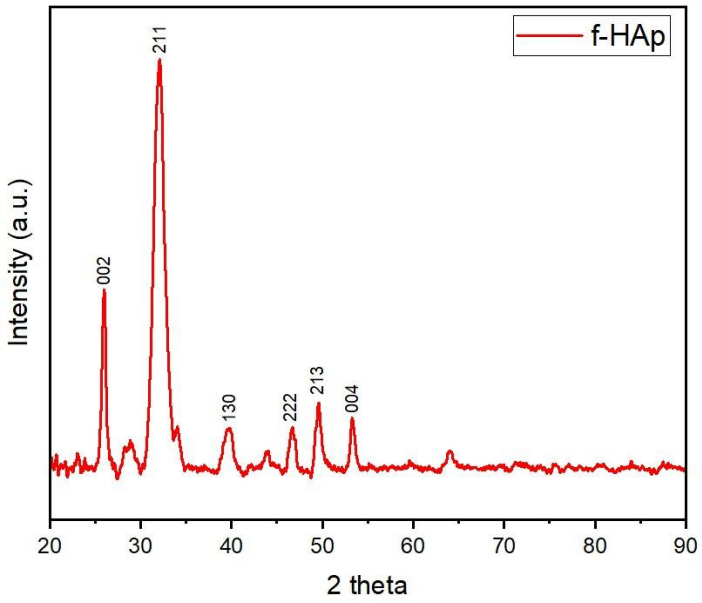

Fig.10. XRD pattern of f-Hap

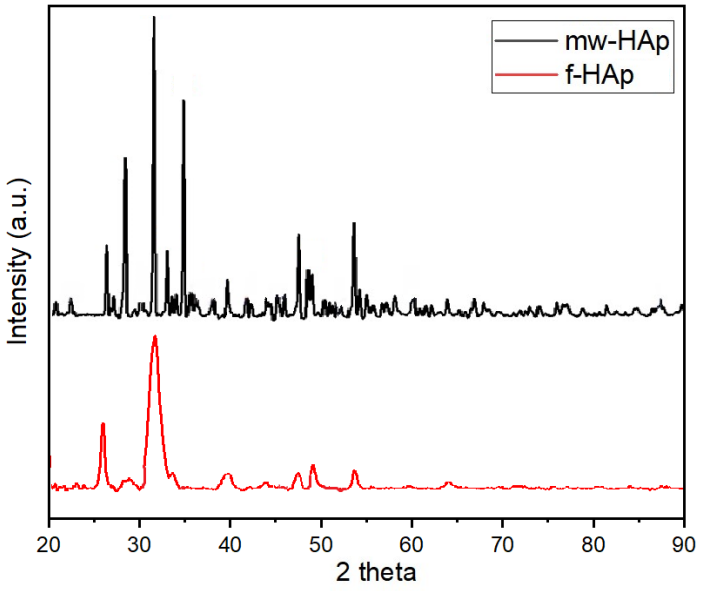

Fig.11. Comparison of XRD pattern between mw-HAp and f-Hap

https://doi.org/10.24191/cos.v12i2.8835

Figure 11 presents a comparative analysis of the XRD patterns for mw-HAp and f-HAp. Both samples exhibit peak positions at similar 2 theta values, indicating a consistent or nearly identical crystalline structure, thereby confirming the presence of a HAp phase in each. The mw-HAP displays more distinct and sharp peak intensities, suggesting a significant crystallinity or phase purity relative to f-HAp. In contrast, the lower peak intensities and broader width in the f-HAp pattern are indicative of a smaller crystallite size and a lower degree of crystallinity, with the broadened peaks pointing to the presence of amorphous material (Hesaraki et al., 2014).

3.4 Fourier Transform Infrared Spectroscopy (FTIR) Analysis

The FTIR spectrum shows information about the molecular structures within both samples. The broad peak seen around the wavenumber 3460 cm^{-1} for FTIR spectra in mw-HAp is indicative of O-H stretching vibration from hydroxyl groups. This peak is broader and more intense than the f-HAp sample, suggesting stronger or more hydrogen bonding, possibly due to a higher level of hydration. The peak around 1640 cm^{-1} in both samples is typically associated with the bending vibrations of (H-O-H), suggesting the presence of water molecules within the sample. A sharp and prominent peak around 1044 cm^{-1} corresponds to the phosphate (PO_4^{3-}) stretching vibrations, a primary constituent of HAp. Peak around 960 cm^{-1} is related to the phosphate (PO_4^{3-}) stretching mode, and it is more pronounced in the mw-HAp sample, indicating a well-defined crystalline phase. Peaks around 600 cm^{-1} and 560 cm^{-1} are due to the bending modes of the phosphate groups, which further confirm the presence of phosphate in the HAp structure. The mw-HAp sample has more pronounced hydroxyl and phosphate peaks compared to the f-HAp sample. Peaks were also seen in the region 1450-1410 cm^{-1} in f-HAp spectra, indicating the bending mode of the C-O bond. This suggests the presence of carbonate group substitution in both mw-HAP and f-HAp lattice (carbonated HAp) (Fig. 12).

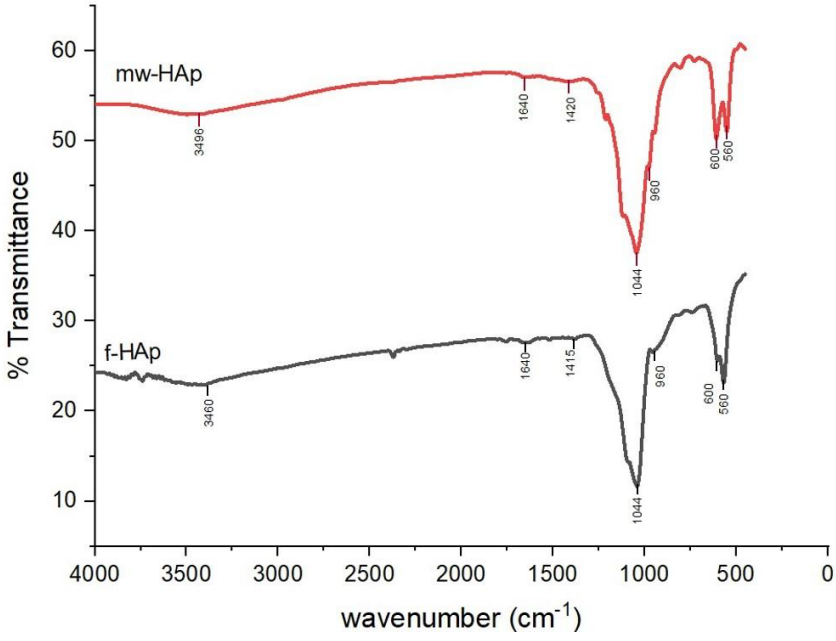

Fig.12. FTIR Spectra of mw-HAp and f-Hap

https://doi.org/10.24191/cos.v12i2.8835

3.5 Morphology and Agglomeration

Particle morphology for mw-HAp and f-HAp are shown in Figures 12 and 13, respectively. Analysis from FESEM shows that mw-HAp depicts a highly ordered morphology characterized by its rounded, nodular formations. These uniform structures exhibit a densely packed arrangement, indicative of a crystalline organization. Porosity was present between the particles. In contrast, f-HAp reveals a disordered, porous, amorphous network with its web-like fibrils and substantial porosity. The determination of pore sizes and interconnectivity is impossible due to overlapping non-homogenous structures of both HAp.

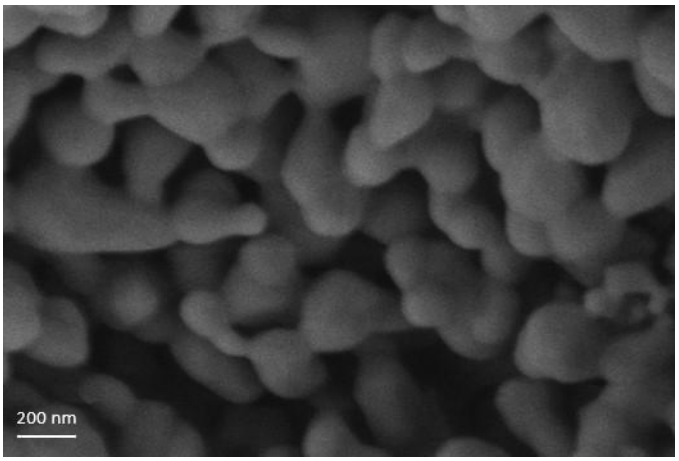

Fig.13. Image of HAp produced by microwave-irradiation method.

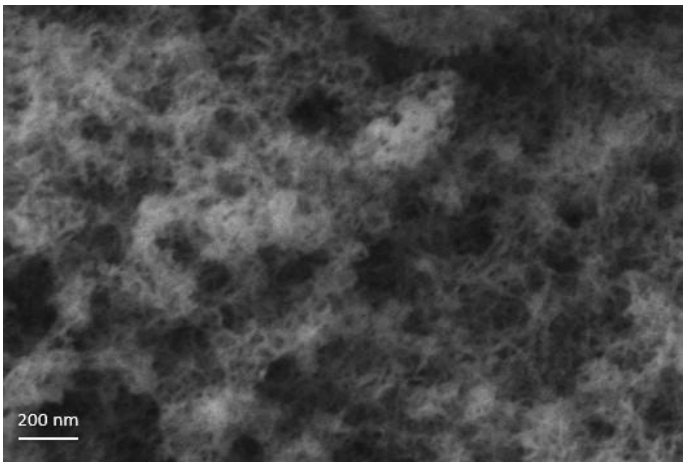

Fig. 14. Image of HAp produced by filtration method

https://doi.org/10.24191/cos.v12i2.8835

4. DISCUSSION

4.1 Synthesis of Hydroxyapatite

Given the pivotal role of HAp in biomedical applications, especially in bone tissue engineering, optimizing its synthesis process is crucial for enhancing its functional qualities. Other than higher purity and more uniform particle sizes and shapes, microwave-assisted synthesis from this study offers several advantages, including reduced reaction times. This research aimed to validate these advantages by systematically comparing the physicochemical properties of the microwave-synthesized HAp with those prepared via traditional routes. The results from this study show that using a domestic microwave was beneficial for producing a new HAp with novel morphology with high crystallinity and validates the findings from the previous studies (Castro et al., 2022; Kalaiselvi et al., 2018). Besides that, mw-HAp synthesis significantly reduced the reaction time, surpassing the time for filtration and washing.

This study made modifications to the microwave power and irradiation duration using precursors akin to those in a prior study. The referenced research by Lamkhao et al. 2019 generated three distinct HAp varieties through filtering, microwave irradiation, and hotplate methods (Lamkhao et al., 2019). The results from this study show that despite using an identical approach for f-HAp production, variations in the Ca/P ratio were observed, hinting at the presence of additional factors that could influence the outcomes. In the current study, variables such as pH, microwave intensity, chemical solution types, stirring duration, and post-synthesis processing were uniformly maintained.

The environment in which HAp is synthesized significantly impacts its chemical and physical characteristics. The choice of atmosphere can profoundly influence the reaction processes, the oxidation states of the components, and the overall purity of the HAp. Moreover, the atmospheric conditions affect the thermal and pressure settings under which the HAp crystals form. For instance, performing the synthesis in a vacuum can promote the development of larger, more well-defined crystals by reducing resistance to mass transfer from the gas phase. Furthermore, employing an inert gas atmosphere, such as nitrogen or argon, is essential for preventing the oxidation of vulnerable elements, thereby ensuring the HAp's desired stoichiometry and purity remain intact (Szterner & Biernat, 2022).

The stirring speed was not specified in the previous study (Lamkhao et al., 2019). The stirring speed affects the interaction between the precursors, which hinges on the availability of Ca^{2+} and PO_4^{3-} ions. An increase in stirring speed enhances the solubility of the precursors, thereby making more ions available for the reaction and reducing particle agglomeration. It was discovered in one investigation that intense stirring led to notable differences in the size and shape of HAp particles. (Le et al., 2014).

In this study, different irradiation times and power were used for several reasons. First, the combustion method involves burning precursors until the desired compound is dried. The temperatures can be very high and difficult to control, leading to non-uniform temperature distribution. This high temperature can result in uneven phase transformations and the development of unwanted phases or defects in the HAp structure. Meanwhile, the irradiation method allows precise control over temperature and heating rate at a short duration, thus ensuring the gradual transformation of precursors into HAp. This ensures uniform crystal growth and phase purity.

Second, the definition of dryness was not specified in the previous study, and the measurement of dryness was also not mentioned. Thirdly, the high temperature leads to the oxidation of the precursors, producing a compound containing calcium oxide, which is not required for bone regeneration. Third, the high temperatures and rapid processing can sometimes result in the decomposition of HAp into other

https://doi.org/10.24191/cos.v12i2.8835

calcium phosphate phases, such as tricalcium phosphate (TCP), which have different properties and may not be desired (Burdusel et al., 2023). In contrast to the irradiation method, by carefully controlling the power, it is possible to avoid the decomposition of HAp and ensure the stability of the HAp phase, which is important for its application in bone regeneration and repair.

4.2 Preliminary Analysis of Calcium-to-Phosphorus Ratio

The theoretical Ca/P ratio for pure HAp is 1.67 (LeGeros, 2008). However, using both methods, this study found that the optimum Ca/P value was 1.8 for mw-HAP and 2.0 for f-HAp, suggesting a deviation from this ideal ratio. The control of chemical composition is a common problem in the synthesis of HAp, often producing a non-stoichiometric calcium phosphate powder. In the chemical synthesis of HAp, other studies studies that use various techniques exhibit a Ca/P ratio ranging from 1.67 to 2.2. This variation is attributed to ion substitutions during chemical reactions, resulting in amorphous structures (Lee et al. 2020; Sawada et al. 2021). Deviations from the stoichiometric value by 1% or 2% are generally considered acceptable (Raynaud et al., 2001).

The deviation in the Ca/P ratio might be attributed to various factors. Contaminants present in the initial materials (calcium and phosphate sources) could introduce extraneous elements into the HAp structure, impacting the Ca/P ratio. Additionally, ionic substitutions within the HAp lattice, such as carbonate substituting for phosphate, resulting in carbonated HAp, or different cations, such as magnesium or strontium taking the place of calcium, may also modify the Ca/P ratio (Le et al., 2014). Ramesh et al. 2007 found that the presence of impurities such as calcium oxide contributed to a Ca/P ratio of more than 1.8 in HAp. It was suggested that the post-synthesis treatment, such as a higher temperature during the sintering process, leads to the oxidation of HAp, thus disrupting the phase stability (Singh et al., 2007). The findings were further supported by Tan and his colleagues, who found calcium oxide inside the calcium-rich HAp. The compound-containing calcium oxide was claimed to alter the mechanical properties of HAp in terms of lower hardness and fracture toughness compared to ideal stoichiometric HAp (Tan et al., 2015). Additionally, the presence of impurities, particularly calcium oxide, in the material composition has been observed to accelerate degradation rates, which may adversely impact the biological environment. (Wang et al., 2003). An elevated Ca/P ratio can be attributed to the presence of impurities, which correspondingly reduced the crystallinity. Nonetheless, the incorporation of certain ion substitutions into HAp does not necessarily lead to detrimental effects. Specifically, carbonate ions, which are naturally found in bone, may enhance bioactivity when present in HAp. This enhancement is likely due to the increased structural resemblance to natural bone (Noor et al., 2020).

The variation in the Ca/P ratio in calcium phosphate compounds affects the crystallinity, particle sizes, porosity and average pore sizes (Ergun et al., 2011). It has been observed that an increase in the Ca/P ratio leads to a diminution in both average particle and pore dimensions. At basic pH, the initial Ca/P ratio influences the crystallization rate. Increasing the Ca/P ratio from 0.2 to 1.0 and then to 5.0 results in particle sizes enlarging from 0.8 nm to 2.0 nm and finally to 4.0 nm, respectively (Hoeher et al., 2021). Similarly, Syafaat et al. 2019 compare the particle size of HAp with a Ca/P ratio of 1.67 to 2.08. They found that increasing the Ca/P ratio produced HAp with larger particle size and higher crystallinity and density. Carbonate groups were also found, indicating the replacement of phosphate groups in higher Ca/P HAp (F.Y. Syafaat, 2019).

Beyond physical and mechanical characteristics, understanding the optimal Ca/P ratio for osteogenesis is crucial when considering HAp for specific applications in bone regeneration. Assessing how variations in the Ca/P ratio affect particle sizes, porosity, and pore dimensions and subsequently influence osteoblastic activity is essential. Research indicates that a Ca/P ratio greater than 2.0 is linked to a reduction in osteoblastic activity by approximately 18% compared to ratios less than 2.0, a phenomenon attributed to

https://doi.org/10.24191/cos.v12i2.8835

the stimulation of nitric oxide production by calcium oxide particles. Conversely, maintaining a Ca/P ratio below 2.0 is beneficial for the enhancement of osteoblastic activity and an increase in osteoblast alkaline phosphatase activity (Liu et al., 2008). However, Ergun et al. (2008) observed the highest osteoblast adhesion at a Ca/P ratio of 2.5, indicating that differences in particle size and morphology might explain the variation in these results (Ergun et al., 2008).

Phosphate ion emission from HAp significantly impacts RANKL-triggered osteoclastogenesis by interfering with the electrostatic interaction between RANKL and RANK. This interference hampers the establishment of a salt bridge between RANKL and RANK, negatively affecting their association and blocking the phosphorylation in subsequent signalling pathways. Adjusting the release of phosphate ions through an increased Ca/P ratio in HAp emerges as a viable approach to regulate osteoclast activity and enhance bone integration. A recent study has verified that elevating the Ca/P ratio in HAp can effectively facilitate RANKL-RANK binding and trigger enhanced NF-κB signalling transduction, leading to intensified osteoclast differentiation. This mechanism has been linked to a significant enhancement in bone healing in vivo, attributed to the dynamic interplay of osteoclasts (X. Wang et al., 2021). Thus, it is important to note that a Ca/P ratio greater than 1.67 is more desirable for bone regenerative materials. This is because amorphous HAp, as opposed to its highly crystalline counterpart, exhibits higher degradation rates, facilitating the release of bone formation agents and promoting osteogenesis more effectively (Jin et al., 2023).

In fact, the Ca/P ratio in humans varies between individuals and different parts of the body. Earlier, the Ca/P ratio in human bone was determined to be 1.67. However, it is crucial to mention that this data primarily comes from studies on non-intact bone. The decrease in the Ca/P ratio could result from the bone harvesting and processing methods, which typically involve using solvents to eliminate collagen, fat, and marrow, followed by calcination that may lead to significant losses of calcium and phosphorus. Contrarily, evidence suggests that the Ca/P ratio in healthy, intact human bone ranges between 2.0 and 2.6 (Loughrill et al., 2017; Tzaphlidou & Zaichick, 2003). This might explain the studies that reported an increased osteoblastic activity when the Ca/P ratio in HAp exceeds 1.67, likely due to its greater resemblance to natural, intact bone (Ergun et al., 2011; Liu et al., 2008).

EDXRF has specific limitations when used to detect HAp composition, mainly due to the nature of HAp itself and its operational principles of EDXRF. EDXRF has limited sensitivity to light elements, such as hydrogen, carbon, oxygen, and nitrogen, which are crucial components of HAp ($Ca_{10}(PO_4)_6(OH)_2$). The technique is more efficient in detecting heavier elements due to their more pronounced X-ray fluorescence. This limitation can hinder the precise analysis of HAp's complete chemical composition, especially since it does not directly measure hydrogen or oxygen (Li et al., 2022). In addition, the quantitative assessment of the chemical composition of the mineral depositions, together with their molecular and structural information, can be challenging, as the accuracy of the results may be affected by factors such as sample preparation and instrument calibration (Zhou et al., 2018). Due to these limitations, it is often advantageous to supplement EDXRF with other analytical techniques, such as X-ray diffraction (XRD) for crystalline structure analysis (discussed in section 4.4) and infrared spectroscopy (discussed in section 4.5) or Raman spectroscopy for organic component analysis, to provide a more detail information regarding the HAp composition and structure (Timchenko et al., 2017).

4.3 X-ray Diffraction Analysis

The peaks produced by powder synthesized by both methods were identified and compared to the reference pattern (ICSD ref: 01-074-0566), and the results best match the expected pattern. This indicates that both samples contain HAp. A slight shift in peak positions was observed, especially in mw-HAp. It was also observed that there was a slight shift in peak positions, especially in mw-HAp. This variation

https://doi.org/10.24191/cos.v12i2.8835

might be due to the different measuring environments, such as pressure, atmosphere and temperature. Additionally, it is worth noting that a minor alteration in the peak variation may also be attributed to residual strain and compositional modifications. (Harrington & Santiso, 2021).

The classification of HAp crystallinity by Lerner et al. relies on the analysis of XRD peaks corresponding to the 211, 112, 300, and 202 plane reflections. The methodology delineates four distinct categories of crystallinity: Category 1 is characterized by the absence of peaks across all four specified reflections; Category 2 is defined by the broad peaks that encompass the aforementioned reflections, including the 002 reflection; Category 3 is marked by the emergence of four approximately defined peaks, alongside weak indications of the 201 and 102 peaks; Category 4 signifies HAp that is relatively well-crystallized, as evidenced by high intensity and distinct peak formations. This classification scheme offers a nuanced framework for assessing the degree of crystallinity in hydroxyapatite samples through specific XRD peak resolutions (Lerner et al., 1991)

The XRD pattern obtained for mw-HAp exhibited sharp peaks at peaks 211, 300, and 202, with some weak evidence of peak 112. Thus, the mw-HAp obtained from this study can be categorized as near category 4, characterised by high intensity, indicating a high crystallinity level. When comparing the XRD pattern of the sample to that of f-HAp, it was observed that the latter exhibited broad and low-intensity peaks at 211 and 300, with a very weak peak at 112 and no peak at all at 002. This characteristic indicates that the f-HAp powder is amorphous and potentially contains significant impurities. The specific applications of each type of HAp might favour different properties; for example, higher crystallinity (mw-HAp) might be preferred for structural applications, while lower crystallinity (f-HAp) might be beneficial for applications requiring higher solubility or bioactivity (Otwinowski & Minor, 1997).

The XRD pattern obtained in this investigation had similarities to those observed in several earlier studies. Lamkhao et al. (2019) employed calcium nitrate tetrahydrate and 85% phosphoric acid as precursors for calcium and phosphate, respectively. The suspensions were subjected to combustion within the microwave until total evaporation occurred. The researchers discovered that the HAp synthesised by microwave-assisted approaches exhibited XRD patterns characterised by notably enhanced sharpness and intensity. Additionally, it was noted by the researchers that HAp acquired using alternative techniques, such as hotplate processing, filtering, and commercially available HAp, exhibited wider and less intense peaks. This observation implies the presence of an amorphous structure. (Lamkhao et al., 2019). The XRD pattern obtained from f-HAp in this study confirms the pattern from the previous study.

The utilization of microwave irradiation in this study confirmed the production of HAp with a superior structure. These phenomena can be attributed to several reasons. In the study by Shaban et al. (2021), they employed identical calcium and phosphate precursors to examine the impact of sintering duration on the HAp generated by the utilisation of a microwave-assisted technique. The XRD pattern revealed that the heat-treatment method successfully eliminated any contaminants present in the resulting sample. It was also observed that an increase in sintering time resulted in the production of higher crystallinity (Shaban et al., 2021). In another study by Amalia et al. (2020), XRD analysis was performed on HAp powder synthesised using microwave irradiation. The researchers specifically examined the impact of irradiation time and pH on the resulting HAp powder. Increasing the duration of irradiation can result in the formation of a significant level of crystallinity. They further concluded that the outcomes were attributable to the phenomenon of atomic diffusion, which is induced by the amplification of microwave energy, leading to heightened rates of vibration and temperature. The application of microwave energy induces a substantial increase in temperature, leading to extensive atom diffusion and thus promoting a high level of crystallisation. (Amalia et al., 2020).

https://doi.org/10.24191/cos.v12i2.8835

X-ray diffractometry is a highly effective methodology employed in characterising HAp and other crystalline substances. However, it is important to acknowledge that this technique has certain limitations. The sample may not exhibit a clear representation in the XRD pattern if it has significant contaminants. Moreover, XRD patterns of HAp often exhibit broad peaks, making it challenging to precisely determine crystal size due to the influence of lattice strain and organic components (Londoño-Restrepo et al., 2019). In this scenario, exploring additional characteristics is necessary to substantiate the results obtained from XRD analysis. Techniques such as Fourier-transform infrared spectroscopy (FTIR) and solid-state magnetic resonance analysis should be employed to further characterise the sample, particularly regarding its phase purity (Murphy et al., 2023).

Additionally, XRD offers insights into the average size of crystallites within a material. However, it may not offer a comprehensive analysis of the distribution of crystallite sizes. In order to obtain a more thorough examination of the distribution and morphology of crystallite size, additional techniques such as transmission electron microscopy (TEM) or scanning electron microscopy (SEM) may be necessary. Moreover, XRD is predominantly utilised as a technique for analysing bulk materials. The provided data may lack comprehensive insights into HAp's surface structure or composition. Surface characterisation may be better suited to employing techniques such as X-ray photoelectron spectroscopy (XPS) and EXDRF (Eric, 2011).

4.4 Fourier Transform Infrared Spectroscopy (FTIR) Analysis

Overall, FTIR spectra confirmed the XRD and EDXRF analysis results regarding the presence of hydroxyl and phosphate groups in both samples, with the presence of impurities contributed by carbonate substitution. However, mw-HAp shows sharper and more defined peaks, which might indicate a higher crystallinity than f-HAp. Two reasons can explain the presence of carbonate. Firstly, during the precipitation method, carbonate ions replaced hydroxyl groups, producing carbonate appetite with reduced crystallinity and precipitate size. Secondly, carbonate ions replace phosphate groups that can only occur in high-temperature methods in the presence of carbon dioxide. The latter type of reaction produces high crystalline materials that can be detected through x-ray diffraction analysis. In addition, carbonate ions can be substituted into hydroxyl and phosphate groups, producing a mixture of both HAp types (Barralet et al., 1998).

The inclusion of carbonate in HAp enhances its similarity to the mineral structure and biological traits of natural bone. Studies have shown that HAp containing carbonate offers improved biocompatibility and a faster resorption rate, making it a more effective material for bone regeneration than pure HAp (Šupová, 2015). The activity of bone cells is also increased with the incorporation of carbonate into HAp. In a study conducted by Germaini et al. in 2017, it was found that osteoblastic cells exhibited higher proliferation rates when in contact with carbonated HAp without adversely affecting the osteogenic molecular pathways. Furthermore, the viability and metabolism of both osteoblasts and osteoclasts were enhanced when exposed to carbonated HAp (Germaini et al., 2017). Hesaraki and colleagues 2014 conducted a study comparing the effects of carbonated HAp to those of pure HAp on mesenchymal stem cells and fibroblasts derived from Winstar rats. The study found enhanced cell growth and differentiation in the carbonate HAp-treated cells. While both forms of HAp showed effective osteoconductivity and biocompatibility for bone healing, pure HAp was found to have a slower resorption rate, which could restrict bone remodelling capabilities (Hesaraki et al., 2014).

Even though FTIR analysis is a well-established method for identifying phosphate and hydroxyl groups in HAp, there are some limitations that need to be considered. The method of sample preparation can significantly affect the FTIR spectra. For example, pressing samples into pellets with KBr can introduce

https://doi.org/10.24191/cos.v12i2.8835

contamination or alter the HAp, potentially affecting the interpretation of the spectra. In addition, FTIR analysis is technique-sensitive; thus, it has limitations in detecting low concentrations of HAp in a mixture (Kamnev et al., 2017). Furthermore, while FTIR can provide qualitative information about the presence of specific functional groups in HAp, quantitative analysis can be challenging. Factors such as the sample's thickness, particle size, and the presence of other compounds can affect the absorbance readings, making it difficult to accurately quantify the components. Finally, the environmental and physical factors, such as the presence of water and carbon dioxide, can interfere with FTIR analysis as the can be adsorbed in the same range as HAp, affecting the spectra. The physical state of HAp, such as crystallinity, can significantly influence the infrared absorption characteristics and potentially mislead the results (Sahadat Hossain & Ahmed, 2023).

4.5 Morphology and Agglomeration

The morphology of HAp particles plays a crucial role in determining their cytotoxicity and the subsequent inflammatory response when interacting with biological systems. The shape and size of HAp particles can significantly affect their interaction with cells, including how cells take up these particles and respond to them. This response is particularly relevant in the context of developing biomaterials for medical applications, where minimizing adverse reactions is essential.

Studies such as those by Motskin et al. (2009), Grandjean-Laquerriere et al. (2005), and Laquerriere et al. (2003) have investigated the impact of micro- and nanoparticles of various materials on the production of inflammatory cytokines. These cytokines, including tumour necrosis factors-α (TNF-α), interleukin-6 (IL-6), and interleukin-18 (IL-18), are key mediators of the inflammatory response. The findings from these studies underscore the significance of particle morphology on cellular responses, highlighting that different shapes and sizes of particles can lead to varying degrees of inflammation and cytotoxicity (Grandjean-Laquerriere et al., 2005; Laquerriere et al., 2003; Motskin et al., 2009). HAp particle cytotoxicity varies considerably and is highly dependent on their physical properties. Zhao et al. (2013) specifically compared the effects of nanosized HAp particles of various shapes, including needle-shaped, plate, sphere, and rod-like structures, on macrophages and human epithelial cells . Their study found that needle- and plate-shaped HAp particles induced the most significant cytotoxic effects. These effects were attributed to higher cellular uptake and agglomeration, which, in turn, increased the phagocytic activity of macrophages. Additionally, exposure to needle- and plate-shaped HAp particles led to unusual morphological changes in macrophages, resulting in aberrant phagocytic activity (Zhao et al., 2013). Building on this, Lebre et al. (2017) expanded the investigation to examine how different HAp shapes and concentrations affect cytokine production by bone marrow dendritic cells, a key immune response component. Their findings revealed that needle-shaped HAp particles, across all tested concentrations, were cytotoxic to dendritic cells, leading to increased interleukin-1β (IL-1β), a pro-inflammatory cytokine.

In contrast, smooth-shaped HAp particles did not induce detectable levels of IL-1β, highlighting the importance of particle shape in dictating biological responses. The in-vivo studies conducted by Lebre et al. further validated these observations, showing that needle-shaped HAp particles, when administered intraperitoneally in mice, caused significant macrophage depletion and decreased mast cells while simultaneously recruiting neutrophils, eosinophils, and monocytes up to seven days post-injection. This prolonged inflammatory response was not observed with spherical HAp particles, suggesting that the morphology of HAp can have a profound impact on the duration and nature of the immune response (Lebre et al., 2017). These studies emphasize the critical role of particle morphology in the design and application of biomaterials. Understanding how specific physical properties of materials, such as shape and size, influence their interaction with biological systems is vital for developing safer and more effective therapeutic tools.

https://doi.org/10.24191/cos.v12i2.8835

This investigation revealed that mw-HAp is characterized by particles of a smooth morphology. Based on these observations, it is postulated that mw-HAp is unlikely to provoke sustained inflammatory responses or exhibit cytotoxicity towards macrophages and dendritic cells. However, this proposition necessitates additional investigation to confirm its validity.

In this research, porosity was observed in both forms of HAp. Porosity affects not just the biological integration and functionality of HAp scaffolds but also their mechanical strength. Optimum pore sizes are essential for the growth of bone tissue into the scaffold, ensuring its fusion with adjacent bone. These pores provide pathways for nutrient and oxygen diffusion to cells within the scaffold, aid in expulsion of metabolic waste, and support revascularization (Abere et al., 2022).

The ideal pore size for bone regeneration has been a topic of debate. Osteoblasts, which are between 20-50 μm in size, require larger pores to penetrate the scaffold and form new bone. This necessity for larger pores is linked to the prerequisite activity of macrophages, which remove bacteria and dead cells, thereby facilitating the infiltration of other cells that contribute to colonization, migration, and vascularization, setting the stage for osteoblast activity (Iviglia et al., 2019). Previous research indicated that pore sizes around 800 μm significantly enhance bone growth, noting that smaller pores tended to be occupied by fibroblasts, while the ingrowth of osteoblastic cells favored larger pores (Roosa et al., 2010). Further studies by Cheng et al. assessed osteoblastic behavior in relation to pore sizes ranging from 250 to 400 μm, finding that larger pores facilitated the development of more mature bone structures, as evidenced by increased levels of osteopontin, collagen type I, and mature bone markers. Additionally, bigger pores were found to promote the formation of new blood vessels, which are crucial for supplying oxygen and nutrients to osteoblastic cells (Cheng et al., 2016). Larger pores offer greater permeability, which is beneficial for cell growth and proliferation. This is because larger pores take longer to become occluded during ongoing growth, providing additional time for bone formation to occur (Kang & Chang, 2018).

On the other hand, O'Brien et al. discovered that a smaller pore size of 95 μm is sufficient for protein adhesion and the initial attachment of cells, noting that micropores of this size offer a greater surface area (Murphy & O'Brien, 2010). Previous research has indicated that while pore sizes greater than 50 μm (referred to as macropores) improve osteogenic properties, the infiltration of cells is limited by smaller pore sizes in in-vitro studies. Conversely, a pore size smaller than 10 μm (termed micropore) increases the surface area, which in turn enhances ion exchange and the adsorption of bone proteins (Morejón et al., 2019).

A. Boccaccio and his team engineered a scaffold with graded porosity aimed at improving bone regeneration and functional stability. This innovative scaffold featured a porous section designed to simulate the soft cancellous bone and a denser section to resemble the hard cortical bone. The results indicated that this gradient scaffold facilitated better bone growth, cell proliferation, and nutrient flow and was more effective at withstanding mechanical forces than scaffolds with consistent porosity (Boccaccio et al., 2016). In a separate study conducted by Sobral et al. in 2011, the ability of mouse osteoblasts to populate a HAp plate with gradient pore sizes was examined. The findings showed that the scaffold with varied pore sizes had a 75% cell seeding efficiency, significantly higher than the 35% efficiency of the scaffold with uniform pore sizes (Sobral et al., 2011). Therefore, scaffolds with heterogeneous pore sizes appear to be more effective for bone regeneration compared to those with uniform pore sizes.

Jang and his team explored how porous and granular HAp influences the ability to regenerate alveolar bone. Findings from 4 to 12 weeks after implantation into the alveolar sockets of mice showed that new bone growth was significantly greater in the case of porous HAp, which had adjustable pore sizes and interconnectedness, as evidenced by the increased occurrence of osteophytes, in comparison to granular HAp (Jang et al., 2017).

https://doi.org/10.24191/cos.v12i2.8835

FESEM utilizes a field emission gun to generate high-resolution images, effectively capturing the surface morphology and microstructure of HAp. However, this technique yields two-dimensional images and primarily offers surface-level details, with internal structures such as pore sizes remaining elusive without sectioning the sample. The magnification limit for FESEM in this investigation is capped at 200 nm, potentially obscuring the true dimensions of HAp particles. Consequently, the study's insights into HAp's internal makeup were constrained. Enhancement of the methodological approach is suggested through the application of high-resolution transmission electron microscopy (HR-TEM), which achieves magnifications down to 1 nanometre, providing a more intricate view of the material's structure. Nonetheless, TEM preparation necessitates the creation of thin sample sections, a process that risks altering the specimen's original condition, for a thorough examination of both the exterior and interior morphology, including porosity and the network of connections within HAp, X-ray Microcomputed Tomography (Micro-CT) is recommended for its superior capability to generate detailed 3D imagery, presenting a comprehensive perspective on the material's architecture (Su et al., 2018).

5. CONCLUSION

This research has provided significant insights into the synthesis process, physicochemical properties, and biological performance of HAp, paving the way for its optimized application in tissue engineering and regenerative medicine. From the results, it can be concluded that all the hypotheses can be accepted except for the antibacterial properties.

Within the limitations of this study, the adoption of microwave-assisted irradiation for synthesizing HAp emerged as a pivotal advancement, showcasing numerous benefits over conventional methods. This innovative approach led to the production of HAp with superior crystallinity and unique morphology and demonstrated efficiency in terms of reduced reaction times. These attributes underscore the potential of microwave-assisted synthesis in improving the quality and functional properties of HAp, making it a more viable option for bone regeneration.

In synthesizing these findings, the study articulates a compelling case for the continued exploration and optimization of HAp's properties for biomedical applications. The research advances our understanding of HAp's synthesis, characterization, and potential applications and lays the groundwork for future investigations aimed at harnessing its capabilities for enhanced bone tissue engineering and regenerative medicine. The multidisciplinary approach, combining materials science, biology, and engineering, underscores the complexity of developing biomaterials that meet the rigorous demands of biomedical applications. As the quest for optimal bone regeneration strategies continues, HAp stands out as a material with significant promise, necessitating further research to fully exploit its potential in improving patient outcomes in bone

The research in the field of HAp can continue to advance, unlocking new potential for this versatile biomaterial in bone tissue engineering and beyond. The convergence of multidisciplinary efforts from materials science, biology, engineering, and clinical medicine will be crucial in overcoming current limitations and harnessing the full potential of HAp in improving patient care and treatment outcomes.

ACKNOWLEDGEMENT

The authors would like to acknowledge the support of the Faculty of Dentistry, Universiti Teknologi MARA, Sungai Buloh campus in providing the facilities required to conduct the work.

FINANCIAL SUPPORT AND SPONSORSHIP

The authors received no financial support for the research, authorship, and/or publication of this article.

CONFLICTS OF INTEREST

Authors declare there are no conflicts of interest.

AUTHORS CONTRIBUTIONS

Nurul Saadah Razali is a specialist periodontist at Mahmoodiah Dental Clinic, Ministry of Health, Johor Bahru, she is the researcher, experimenter and writer of this published article

Luay Thanoon Younis is associate professor at the Faculty of Dentistry, UiTM, Sungai Buloh campus. He is the writer, and the main supervisor of the research related to the topic of this article.

Muhammad Hilmi Zainal Ariffin is a lecturer at the Faculty of Dentistry, UiTM, Sungai Buloh campus and co-supervisor of the the research related to the topic of this article.

Fara Fariza Zahar is a medical laboratory technologist at the Faculty of Dentistry, UiTM, Sungai Buloh campus participated in laboratory research related to the topic of this article.

REFERENCES

Abere, D., Ojo, S., Oyatogun, G., Paredes-Epinosa, M., Niluxsshun, M., & Hakami, A. (2022). Mechanical and morphological characterization of nano-hydroxyapatite (nHA) for bone regeneration: A mini review. *Biomedical Engineering Advances*, *4*, 100056. https://doi.org/10.1016/j.bea.2022.100056.

Amalia, T., Ayat, N., & Sari, Y. (2020). Synthesis of Hidroxyapatite Using Microwave Irradiation and Sintering with Variation pH and Time. *Journal of Physics: Conference Series*, *1505*, 012063. https://doi.org/10.1088/1742-6596/1505/1/012063.

Barralet, J., Best, S., & Bonfield, W. (1998). Carbonate substitution in precipitated hydroxyapatite: an investigation into the effects of reaction temperature and bicarbonate ion concentration. *J Biomed Mater Res*, *41*(1), 79-86. https://doi.org/10.1002/(sici)1097-4636(199807)41:1<79::aid-jbm10>3.0.co;2-c.

Bilton, M. (2012). *Nanoparticulate hydroxyapatite and calcium-based CO2 sorbents*.

Boccaccio, A., Uva, A. E., Fiorentino, M., Mori, G., & Monno, G. (2016). Geometry Design Optimization of Functionally Graded Scaffolds for Bone Tissue Engineering: A Mechanobiological Approach. *PLoS One*, *11*(1), e0146935. https://doi.org/10.1371/journal.pone.0146935.

Burdusel, A. C., Neacsu, I. A., Birca, A. C., Chircov, C., Grumezescu, A. M., Holban, A. M., Curutiu, C., Ditu, L. M., Stan, M., & Andronescu, E. (2023). Microwave-Assisted Hydrothermal Treatment of Multifunctional Substituted Hydroxyapatite with Prospective Applications in Bone Regeneration. *J Funct Biomater*, *14*(7). https://doi.org/10.3390/jfb14070378.

Castro, M. A. M., Portela, T. O., Correa, G. S., Oliveira, M. M., Rangel, J. H. G., Rodrigues, S. F., & Mercury, J. M. R. (2022). Synthesis of hydroxyapatite by hydrothermal and microwave irradiation methods from biogenic calcium source varying pH and synthesis time. *Boletín de la Sociedad Española de Cerámica y Vidrio*, *61*(1), 35-41. https://doi.org/https://doi.org/10.1016/j.bsecv.2020.06.003.

Cheng, M., Wahafu, T., Jiang, G., Liu, W., Qiao, Y., Peng, X., Cheng, T., Zhang, X., He, G., & Liu, X. (2016). A novel open-porous magnesium scaffold with controllable microstructures and properties for bone regeneration. *Scientific Reports*, *6*(1), 24134.

Cortellini, P., & Tonetti, M. S. (2015). Clinical concepts for regenerative therapy in intrabony defects. *Periodontol 2000*, *68*(1), 282-307. https://doi.org/10.1111/prd.12048.

Ergun, C., Evis, Z., Webster, T. J., & Sahin, F. C. (2011). Synthesis and microstructural characterization of nano-size calcium phosphates with different stoichiometry. *Ceramics International*, *37*, 971-977.

Ergun, C., Liu, H., Webster, T. J., Olcay, E., Yilmaz, S., & Sahin, F. C. (2008). Increased osteoblast adhesion on nanoparticulate calcium phosphates with higher Ca/P ratios. *J Biomed Mater Res A*, *85*(1), 236-241. https://doi.org/10.1002/jbm.a.31555.

Eric, M. R. (2011). Hydroxyapatite-Based Materials: Synthesis and Characterization. In F.-R. Reza (Ed.), *Biomedical Engineering* (pp. Ch. 4). IntechOpen. https://doi.org/10.5772/19123.

F.Y. Syafaat, Y. Y. (2019). Influence of Ca/P concentration on Hydroxyapatite (HAp) from Asian Moon Scallop Shell (Amusium Pleuronectes). *International Journal of Nanoelectronics and Materials*, *12*(No. 3), Pages 357 to 362.

García-Baños, B., Reinosa, J. J., Peñaranda-Foix, F. L., Fernández, J. F., & Catalá-Civera, J. M. (2019). Temperature Assessment Of Microwave-Enhanced Heating Processes. *Sci Rep*, *9*(1), 10809. https://doi.org/10.1038/s41598-019-47296-0.

Germaini, M. M., Detsch, R., Grünewald, A., Magnaudeix, A., Lalloue, F., Boccaccini, A. R., & Champion, E. (2017). Osteoblast and osteoclast responses to A/B type carbonate-substituted hydroxyapatite ceramics for bone regeneration. *Biomed Mater*, *12*(3), 035008. https://doi.org/10.1088/1748-605X/aa69c3.

Grandjean-Laquerriere, A., Laquerriere, P., Guenounou, M., Laurent-Maquin, D., & Phillips, T. M. (2005). Importance of the surface area ratio on cytokines production by human monocytes in vitro induced by various hydroxyapatite particles. *Biomaterials*, *26*(15), 2361-2369. https://doi.org/10.1016/j.biomaterials.2004.07.036.

Harrington, G., & Santiso, J. (2021). Back-to-Basics tutorial: X-ray diffraction of thin films. *Journal of Electroceramics*, *47*, 1-23. https://doi.org/10.1007/s10832-021-00263-6.

Hesaraki, S., Nazarian, H., Pourbaghi-Masouleh, M., & Borhan, S. (2014). Comparative study of mesenchymal stem cells osteogenic differentiation on low-temperature biomineralized nanocrystalline carbonated hydroxyapatite and sintered hydroxyapatite. *J Biomed Mater Res B Appl Biomater*, *102*(1), 108-118. https://doi.org/10.1002/jbm.b.32987.

Hoeher, A. J., Mergelsberg, S. T., Borkiewicz, O. J., & Michel, F. M. (2021). Impacts of Initial Ca/P on Amorphous Calcium Phosphate. *Crystal Growth & Design*, *21*(7), 3736-3745. https://doi.org/10.1021/acs.cgd.1c00058.

Islam, M. S., Abdulla-Al-Mamun, M., Khan, A., & Todo, M. (2020). Excellency of Hydroxyapatite Composite Scaffolds for Bone Tissue Engineering. *Biomaterials*.

Iviglia, G., Kargozar, S., & Baino, F. (2019). Biomaterials, Current Strategies, and Novel Nano-Technological Approaches for Periodontal Regeneration. *Journal of Functional Biomaterials*, *10*(1), 3. https://www.mdpi.com/2079-4983/10/1/3.

Jang, S. J., Kim, S. E., Han, T. S., Son, J. S., Kang, S. S., & Choi, S. H. (2017). Bone Regeneration of Hydroxyapatite with Granular Form or Porous Scaffold in Canine Alveolar Sockets. *In Vivo*, *31*(3), 335-341. https://doi.org/10.21873/invivo.11064.

Jin, P., Liu, L., Cheng, L., Chen, X., Xi, S., & Jiang, T. (2023). Calcium-to-phosphorus releasing ratio affects osteoinductivity and osteoconductivity of calcium phosphate bioceramics in bone tissue engineering. *BioMedical Engineering OnLine*, *22*(1), 12. https://doi.org/10.1186/s12938-023-01067-1.

Kalaiselvi, V., Mathammal, R., Vijayakumar, S., & Vaseeharan, B. (2018). Microwave assisted green synthesis of Hydroxyapatite nanorods using Moringa oleifera flower extract and its antimicrobial applications. *International Journal of Veterinary Science and Medicine*, *6*(2), 286-295. https://doi.org/https://doi.org/10.1016/j.ijvsm.2018.08.003.

Kamnev, A., Tugarova, A., Dyatlova, Y., Tarantilis, P., Grigoryeva, O., Fainleib, A., & Luca, S. (2017). Methodological effects in Fourier transform infrared (FTIR) spectroscopy: Implications for structural analyses of biomacromolecular samples. *Spectrochimica Acta Part A: Molecular and Biomolecular Spectroscopy*, *193*. https://doi.org/10.1016/j.saa.2017.12.051.

Kang, Y., & Chang, J. (2018). Channels in a porous scaffold: a new player for vascularization. *Regen Med*, *13*(6), 705-715. https://doi.org/10.2217/rme-2018-0022.

Kattimani, V. S., Kondaka, S., & Lingamaneni, K. P. (2016). Hydroxyapatite–-Past, Present, and Future in Bone Regeneration. *Bone and Tissue Regeneration Insights*, *7*, BTRI.S36138. https://doi.org/10.4137/btri.S36138.

Kattimani, V. S., Prathigudupu, R. S., Jairaj, A., Khader, M. A., Rajeev, K., & Khader, A. A. (2019). Role of Synthetic Hydroxyapatite-In Socket Preservation: A Systematic Review and Meta-analysis. *J Contemp Dent Pract*, *20*(8), 987-993.

Kim, S., Ryu, H.-S., Jung, H., & Hong, K. (2004). Influence of Ca/P ratios of starting solutions on the crystallization of amorphous calcium phosphate to hydroxyapatite. *Metals and Materials International*, *10*, 171-175. https://doi.org/10.1007/BF03027322.

Kolmas, J., Groszyk, E., & Kwiatkowska-Różycka, D. (2014). Substituted Hydroxyapatites with Antibacterial Properties. *BioMed Research International*, *2014*, 178123. https://doi.org/10.1155/2014/178123.

Lamkhao, S., Phaya, M., Jansakun, C., Chandet, N., Thongkorn, K., Rujijanagul, G., Bangrak, P., & Randorn, C. (2019). Synthesis of Hydroxyapatite with Antibacterial Properties Using a Microwave-Assisted Combustion Method. *Scientific Reports*, *9*(1), 4015. https://doi.org/10.1038/s41598-019-40488-8.

Laquerriere, P., Grandjean-Laquerriere, A., Jallot, E., Balossier, G., Frayssinet, P., & Guenounou, M. (2003). Importance of hydroxyapatite particles characteristics on cytokines production by human monocytes in vitro. *Biomaterials*, *24*(16), 2739-2747. https://doi.org/10.1016/s0142-9612(03)00089-9.

Larsson, L., Decker, A. M., Nibali, L., Pilipchuk, S. P., Berglundh, T., & Giannobile, W. V. (2015). Regenerative Medicine for Periodontal and Peri-Implant Diseases. *Journal of Dental Research*. https://doi.org/10.1177/0022034515618887.

Le, B., Bui, L., & Othman, R. (2014). Carbonate Hydroxyapatite and Silicon-Substituted Carbonate Hydroxyapatite: Synthesis, Mechanical Properties, and Solubility Evaluations. *TheScientificWorldJournal*, *2014*, 969876. https://doi.org/10.1155/2014/969876.

Lebre, F., Sridharan, R., Sawkins, M. J., Kelly, D. J., O'Brien, F. J., & Lavelle, E. C. (2017). The shape and size of hydroxyapatite particles dictate inflammatory responses following implantation. *Sci Rep*, *7*(1), 2922. https://doi.org/10.1038/s41598-017-03086-0.

LeGeros, R. Z. (2008). Calcium phosphate-based osteoinductive materials. *Chem Rev*, *108*(11), 4742-4753. https://doi.org/10.1021/cr800427g.

Lerner, E., Sarig, S., & Azoury, R. (1991). Enhanced maturation of hydroxyapatite from aqueous solutions using microwave irradiation. *Journal of Materials Science: Materials in Medicine*, *2*, 138-141.

Li, F., Meng, L., Ding, W., Wang, J., & ge, L. (2022). Review of energy-dispersive X-ray fluorescence on food elements detection. *X-Ray Spectrometry*, *51*. https://doi.org/10.1002/xrs.3279.

Liu, H., Yazici, H., Ergun, C., Webster, T. J., & Bermek, H. (2008). An in vitro evaluation of the Ca/P ratio for the cytocompatibility of nano-to-micron particulate calcium phosphates for bone regeneration. *Acta Biomater*, *4*(5), 1472-1479. https://doi.org/10.1016/j.actbio.2008.02.025.

Londoño-Restrepo, S. M., Jeronimo-Cruz, R., Millán-Malo, B. M., Rivera-Muñoz, E. M., & Rodriguez-García, M. E. (2019). Effect of the Nano Crystal Size on the X-ray Diffraction Patterns of Biogenic Hydroxyapatite from Human, Bovine, and Porcine Bones. *Scientific Reports*, *9*(1), 5915. https://doi.org/10.1038/s41598-019-42269-9.

Loughrill, E., Wray, D., Christides, T., & Zand, N. (2017). Calcium to phosphorus ratio, essential elements and vitamin D content of infant foods in the UK: Possible implications for bone health. *Matern Child Nutr*, *13*(3). https://doi.org/10.1111/mcn.12368.

Meyle, J., & Chapple, I. (2015). Molecular aspects of the pathogenesis of periodontitis. *Periodontol 2000*, *69*(1), 7-17. https://doi.org/10.1111/prd.12104.

Morejón, L., Delgado, J. A., Antunes Ribeiro, A., Varella de Oliveira, M., Mendizábal, E., García, I., Alfonso, A., Poh, P., Van Griensven, M., & Balmayor, E. R. (2019). Development, characterization and in vitro biological properties of scaffolds fabricated from calcium phosphate nanoparticles. *International journal of molecular sciences*, *20*(7), 1790.

Motskin, M., Wright, D. M., Muller, K., Kyle, N., Gard, T. G., Porter, A. E., & Skepper, J. N. (2009). Hydroxyapatite nano and microparticles: correlation of particle properties with cytotoxicity and biostability. *Biomaterials*, *30*(19), 3307-3317. https://doi.org/10.1016/j.biomaterials.2009.02.044.

Murphy, B., Baez, J., & Morris, M. A. (2023). Characterizing Hydroxyapatite Deposited from Solution onto Novel Substrates in Terms of Growth Mechanism and Physical Chemical Properties. *Materials Proceedings*, *14*(1), 34. https://www.mdpi.com/2673-4605/14/1/34.

Murphy, C. M., & O'Brien, F. J. (2010). Understanding the effect of mean pore size on cell activity in collagen-glycosaminoglycan scaffolds. *Cell adhesion & migration*, *4*(3), 377-381.

Noor, M., Afandi, N., Noor, A. F. M., & Ismail, Y. M. B. (2020). Effect of Carbonate to Phosphate Molar Ratios on the Physico-Chemical Properties of Carbonated Hydroxyapatite Nanopowder.

Otwinowski, Z., & Minor, W. (1997). Processing of X-ray diffraction data. *Methods in enzymology*, *276C*, 307-326. https://doi.org/10.1016/S0076-6879(97)76066-X.

Peak, D. (2005). FOURIER TRANSFORM INFRARED SPECTROSCOPY. In D. Hillel (Ed.), *Encyclopedia of Soils in the Environment* (pp. 80-85). Elsevier. https://doi.org/https://doi.org/10.1016/B0-12-348530-4/00174-0.

Rajula, M. P. B., Narayanan, V., Venkatasubbu, G. D., Mani, R. C., & Sujana, A. (2021). Nano-hydroxyapatite: A Driving Force for Bone Tissue Engineering. *J Pharm Bioallied Sci*, *13*(Suppl 1), S11-s14. https://doi.org/10.4103/jpbs.JPBS_683_20.

Raynaud, S., Champion, E., Bernache-Assollant, D., & Laval, J. (2001). Determination of Calcium/Phosphorus Atomic Ratio of Calcium Phosphate Apatites Using X-Ray Diffractometry. *Journal of the American Ceramic Society*, *84*, 359-366. https://doi.org/10.1111/j.1151-2916.2001.tb00663.x.

Roosa, S. M. M., Kemppainen, J. M., Moffitt, E. N., Krebsbach, P. H., & Hollister, S. J. (2010). The pore size of polycaprolactone scaffolds has limited influence on bone regeneration in an in vivo model. *Journal of Biomedical Materials Research Part A: An Official Journal of The Society for Biomaterials, The Japanese Society for Biomaterials, and The Australian Society for Biomaterials and the Korean Society for Biomaterials*, *92*(1), 359-368.

Sahadat Hossain, M., & Ahmed, S. (2023). FTIR spectrum analysis to predict the crystalline and amorphous phases of hydroxyapatite: a comparison of vibrational motion to reflection. *RSC Adv*, *13*(21), 14625-14630. https://doi.org/10.1039/d3ra02580b.

Sano, T., Kuraji, R., Miyashita, Y., Yano, K., Kawanabe, D., & Numabe, Y. (2023). Biomaterials for Alveolar Ridge Preservation as a Preoperative Procedure for Implant Treatment: History and Current Evidence. *Bioengineering*, *10*(12), 1376. https://www.mdpi.com/2306-5354/10/12/1376.

Sanz-Sánchez, I., Ortiz-Vigón, A., Sanz-Martín, I., Figuero, E., & Sanz, M. (2015). Effectiveness of Lateral Bone Augmentation on the Alveolar Crest Dimension: A Systematic Review and Meta-analysis. *J Dent Res*, *94*(9 Suppl), 128s-142s. https://doi.org/10.1177/0022034515594780.

Shaban, N. Z., Kenawy, M. Y., Taha, N. A., Abd El-Latif, M. M., & Ghareeb, D. A. (2021). Synthesized Nanorods Hydroxyapatite by Microwave-Assisted Technology for In Vitro Osteoporotic Bone Regeneration through Wnt/β-Catenin Pathway. *Materials (Basel)*, *14*(19). https://doi.org/10.3390/ma14195823.

Singh, R., Tan, C., Abd Shukor, M., Sopyan, I., & Teng, W. (2007). The influence of Ca/P ratio on the properties of hydroxyapatite bioceramics. *Proc SPIE*, *6423*. https://doi.org/10.1117/12.779890.

Sobral, J. M., Caridade, S. G., Sousa, R. A., Mano, J. F., & Reis, R. L. (2011). Three-dimensional plotted scaffolds with controlled pore size gradients: Effect of scaffold geometry on mechanical performance and cell seeding efficiency. *Acta Biomater*, *7*(3), 1009-1018. https://doi.org/10.1016/j.actbio.2010.11.003.

Sudarsanan, K., & Young, R. A. (1969). Significant precision in crystal structural details. Holly Springs hydroxyapatite. *Acta Crystallographica Section B*, *25*(8), 1534-1543. https://doi.org/https://doi.org/10.1107/S0567740869004298.

Šupová, M. (2015). Substituted hydroxyapatites for biomedical applications: A review. *Ceramics International*, *41*. https://doi.org/10.1016/j.ceramint.2015.03.316.

Szterner, P., & Biernat, M. (2022). The Synthesis of Hydroxyapatite by Hydrothermal Process with Calcium Lactate Pentahydrate: The Effect of Reagent Concentrations, pH, Temperature, and Pressure. *Bioinorg Chem Appl*, *2022*, 3481677. https://doi.org/10.1155/2022/3481677.

Tan, C. Y., Singh, R., Teh, Y. C., Tan, Y. M., & Yap, B. K. (2015). The Effects of Calcium-to-Phosphorus Ratio on the Densification and Mechanical Properties of Hydroxyapatite Ceramic. *International Journal of Applied Ceramic Technology*, *12*(1), 223-227. https://doi.org/https://doi.org/10.1111/ijac.12249.

Timchenko, P., Timchenko, E., Pisareva, E., Vlasov, M., Red'kin, N., & Frolov, O. (2017). Spectral analysis of allogeneic hydroxyapatite powders. *Journal of Physics: Conference Series*, *784*, 012060. https://doi.org/10.1088/1742-6596/784/1/012060

Tzaphlidou, M., & Zaichick, V. (2003). Calcium, Phosphorus, Calcium-Phosphorus Ratio in Rib Bone of Healthy Humans. *Biological trace element research*, *93*, 63-74. https://doi.org/10.1385/BTER:93:1-3:63.

Wang, H., Lee, J. K., Moursi, A., & Lannutti, J. J. (2003). Ca/P ratio effects on the degradation of hydroxyapatite in vitro. *J Biomed Mater Res A*, *67*(2), 599-608. https://doi.org/10.1002/jbm.a.10538.

Wang, P., Zhao, L., Liu, J., Weir, M. D., Zhou, X., & Xu, H. H. K. (2014). Bone tissue engineering via nanostructured calcium phosphate biomaterials and stem cells. *Bone Research*, *2*(1), 14017. https://doi.org/10.1038/boneres.2014.17.

Wang, X., Yu, Y., Ji, L., Geng, Z., Wang, J., & Liu, C. (2021). Calcium phosphate-based materials regulate osteoclast-mediated osseointegration. *Bioact Mater*, *6*(12), 4517-4530. https://doi.org/10.1016/j.bioactmat.2021.05.003.

Zhao, X., Ng, S., Heng, B. C., Guo, J., Ma, L., Tan, T. T., Ng, K. W., & Loo, S. C. (2013). Cytotoxicity of hydroxyapatite nanoparticles is shape and cell dependent. *Arch Toxicol*, *87*(6), 1037-1052. https://doi.org/10.1007/s00204-012-0827-1.

Zhou, X., Liu, D., Bu, H., Deng, L., Liu, H., Yuan, P., Du, P., & Song, H. (2018). XRD-based quantitative analysis of clay minerals using reference intensity ratios, mineral intensity factors, Rietveld, and full pattern summation methods: A critical review. *Solid Earth Sciences*, *3*(1), 16-29. https://doi.org/https://doi.org/10.1016/j.sesci.2017.12.002.